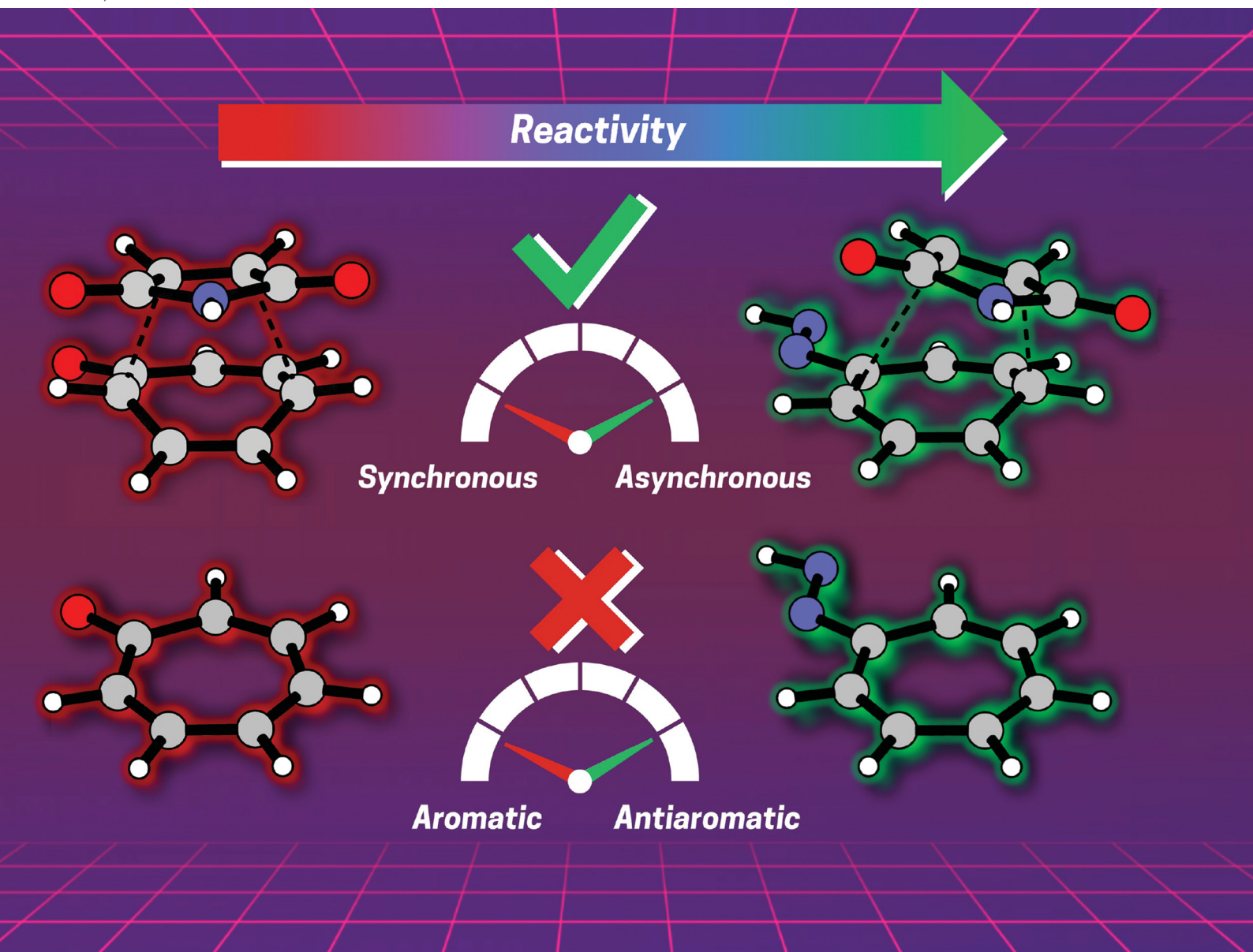


# ChemComm

Chemical Communications

rsc.li/chemcomm



ISSN 1359-7345

**COMMUNICATION**

Pascal Vermeeren, Trevor A. Hamlin *et al.*  
Not antiaromaticity gain, but increased asynchronicity  
enhances the Diels–Alder reactivity of tropone



Cite this: *Chem. Commun.*, 2023, 59, 3703

Received 3rd February 2023,  
Accepted 27th February 2023

DOI: 10.1039/d3cc00512g

rsc.li/chemcomm

# Not antiaromaticity gain, but increased asynchronicity enhances the Diels–Alder reactivity of tropone†

Eveline H. Tiekink, , Pascal Vermeeren \* and Trevor A. Hamlin \*

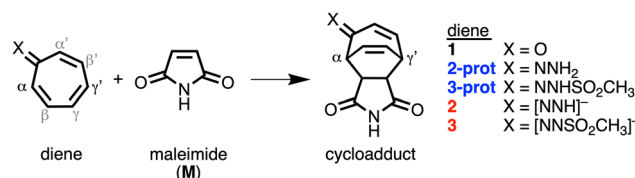
**Tropone is an unreactive diene in normal electron demand Diels–Alder reactions, but it can be activated via carbonyl umpolung by using hydrazone ion analogs. Recently, the higher reactivity of hydrazone ion analogs was ascribed to a raised HOMO energy induced by antiaromaticity (L. J. Karas, A. T. Campbell, I. V. Alabugin and J. I. Wu, *Org. Lett.*, 2020, 22, 7083). We show that this is incorrect, and that the activation barrier is lowered by increased asynchronicity.**

The cycloaddition reactivity of tropone is well documented in literature, although its use as a diene in normal electron demand Diels–Alder reactions is rare.<sup>1</sup> The low reactivity of tropone can be circumvented by reversing the polarity of the carbonyl group (umpolung), *e.g.*, by converting tropone into its hydrazone analog. In 1985, Kajigaeshi *et al.* showed the synthetic power of tropone hydrazones in cycloaddition reactions.<sup>2</sup> Recently, Karas *et al.* studied hydrazone analogs where the carbonyl oxygen of tropone was replaced by =NNH<sub>2</sub> (**2-prot**), =NNHSO<sub>2</sub>CH<sub>3</sub> (**3-prot**) and their anions (**2** and **3**, respectively, Scheme 1).<sup>3</sup> They attributed the accelerated reactivity of the hydrazone analogs to their antiaromaticity, which destabilizes the HOMO and leads to a smaller, more favorable normal electron demand (NED) gap. This *antiaromaticity-induced HOMO-raising strategy* is frequently evoked in organic synthesis.<sup>4</sup>

Herein, we confirm that HOMO-raising enhances the normal electron demand interaction, but simultaneously the LUMO-raising weakens the inverse electron demand (IED) interaction to the same extent. *These two effects effectively cancel each other!* Instead, we trace the accelerated reactivity of hydrazone analogs of tropone back to the increased asynchronicity of the Diels–Alder (DA) reaction mode. Similar conclusions were

found by us and others when studying catalyzed DA reactions.<sup>5</sup> In this work, we challenge the frequently used *antiaromaticity-induced HOMO-raising rationale*. We computationally studied the DA reaction between maleimide and tropone (**1**) and hydrazone analogs **2-prot**, **2**, **3-prot**, and **3** (Scheme 1) using the activation strain model (ASM)<sup>6</sup> with a matching energy decomposition analysis (EDA)<sup>7</sup> and quantitative Kohn–Sham molecular orbital theory.<sup>8</sup> All calculations were conducted using the Amsterdam Modeling Suite (AMS2021.104).<sup>9</sup> Stationary points were optimized at ZORA-BP86-D3(BJ)/TZ2P.<sup>10</sup> Activation strain<sup>6</sup> and energy decomposition analyses<sup>7</sup> were performed at ZORA-ωB97X-D/TZ2P<sup>11</sup> using PyFrag 2019.<sup>12</sup> See the ESI† for computational details.

First, we investigate the reaction profiles of the DA reactions between **M** and **1**, **2-prot**, **2**, **3-prot**, and **3**, by inspecting the electronic activation energies of these reactions (Table 1). Our computed trend in electronic activation barriers is identical to the findings of Karas *et al.* (Table S1, ESI†).<sup>3,13</sup> The activation barrier of the DA reaction with **1** is 24.3 kcal mol<sup>−1</sup> and it increases when reacting to the weakly antiaromatic<sup>3</sup> **2-prot** and **3-prot** to 25.1 kcal mol<sup>−1</sup> and 28.7 kcal mol<sup>−1</sup>, respectively. *Interesting to see that dearomatizing tropone does not always lead to enhanced reactivity.* Only upon deprotonation, the tropone hydrazones become more reactive and the activation barrier lowers to −4.8 kcal mol<sup>−1</sup> and 9.4 kcal mol<sup>−1</sup> for **2** and **3**, respectively. We, therefore, solely focus on the enhanced reactivity of **2** and **3** compared to **1**. Changing the diene also modifies the DA reaction mode as both **1** and **3** follow a



**Scheme 1** The studied Diels–Alder reaction between maleimide (**M**) and diene **1**, **2-prot**, **2**, **3-prot**, and **3**.

Department of Theoretical Chemistry, Amsterdam Institute of Molecular and Life Sciences (AIMMS), Amsterdam Center for Multiscale Modeling (ACMM), Vrije Universiteit Amsterdam, De Boelelaan 1083, Amsterdam 1081 HV, The Netherlands. E-mail: p.vermeeren@vu.nl, t.a.hamlin@vu.nl

† Electronic supplementary information (ESI) available: Additional computational results; computational details; Cartesian coordinates, energies, and the number of imaginary frequencies of all stationary points. See DOI: <https://doi.org/10.1039/d3cc00512g>



**Table 1** Electronic energies ( $\Delta E$ ) of the stationary points (in kcal mol<sup>-1</sup>) for the Diels–Alder reactions between **M** and **1**, **2-prot**, **2**, **3-prot**, and **3**<sup>ab</sup>

Diene	RC	TS1	INT	TS2	P
<b>1</b>	-0.7	24.3			-29.3
<b>2-prot</b>	0.4	25.1			-32.1
<b>3-prot</b>	2.6	28.7			-26.5
<b>2</b>	-10.0	-4.8	-15.1	-13.3	-39.6
<b>3</b>	-5.9	9.4			-37.2

<sup>a</sup> Computed at ZORA- $\omega$ B97X-D/TZ2P//ZORA-BP86-D3(BJ)/TZ2P.<sup>b</sup> See Fig. S1 and Table S1 for the transition state structures and Gibbs free energies (ESI).

concerted asynchronous reaction mode, whereas the DA reaction of **2** goes stepwise. For **1**, although in one reaction step, the C–C <sub>$\alpha$</sub>  bond at the  $\alpha$ -position of **1** is formed ahead of the second C–C <sub>$\gamma'$</sub>  bond at the  $\gamma'$ -position. However, for both **2** and **3**, the C–C <sub>$\gamma'$</sub>  bond forms ahead of the C–C <sub>$\alpha$</sub>  bond. Insight into the differences in asynchronicity and order of bond formation are provided in the ESI.<sup>†</sup>

Next, the physical factors behind the enhanced reactivity of the DA reaction are elucidated using the activation strain model (ASM).<sup>6</sup> The ASM analyzes the cost to deform the original reactants and their ability to interact by decomposing the electronic energy ( $\Delta E$ ) into the strain energy ( $\Delta E_{\text{strain}}$ ) and the interaction energy ( $\Delta E_{\text{int}}$ ). We focus on explaining the origin of the lower activation barrier associated with the DA reaction of **2** compared to the DA reaction of **1**. Table 2 shows the results from the activation strain analysis performed at consistent TS-like geometries where the shorter forming bond between **M** and the diene C<sub>M</sub>...C<sub>diene</sub> is 2.160 Å.<sup>14</sup> The same conclusions emerge from the analysis along the entire reaction coordinate and of the DA reaction with **3** in comparison to **1** (Fig. S2–S5, ESI<sup>†</sup>). The accelerated reactivity of **2** compared to **1** originates from a combination of less destabilizing  $\Delta E_{\text{strain}}$ , 33.0 kcal mol<sup>-1</sup> for **1** to 21.2 kcal mol<sup>-1</sup> for **2**, and more stabilizing  $\Delta E_{\text{int}}$ , from -8.7 kcal mol<sup>-1</sup> for **1** to -24.5 kcal mol<sup>-1</sup> for **2** (Table 2). The lower  $\Delta E_{\text{strain}}$  of the DA reaction of **2** compared to **1** is caused by the higher degree of asynchronicity of this reaction, that is, a larger difference between the newly forming C...C bond lengths. At a consistent geometry, the difference between the two newly forming C–C bonds are  $\Delta r_{\text{C} \cdots \text{C}} = 0.16$  Å for **1** and  $\Delta r_{\text{C} \cdots \text{C}} = 1.09$  Å for **2** (Fig. 1c). The more asynchronous the reaction, the lower the degree of deformation of the reactants in the saddle-point region of the reaction's PES since one C...C bond forms behind the other C...C bond, resulting in a less destabilizing  $\Delta E_{\text{strain}}$ .<sup>15</sup>

**Table 2** Energy decomposition analysis terms (in kcal mol<sup>-1</sup>) of the Diels–Alder reactions between **M** and **1** and **2**<sup>a</sup>

Diene	$\Delta E$	$\Delta E_{\text{strain}}$	$\Delta E_{\text{int}}$	$\Delta V_{\text{elstat}}$	$\Delta E_{\text{Pauli}}$	$\Delta E_{\text{oi}}$
<b>1</b>	24.3	33.0	-8.7	-48.6	98.0	-58.1
<b>2</b>	-3.3	21.2	-24.0	-51.5	83.4	-55.9

<sup>a</sup> Computed at consistent TS-like geometries (C<sub>M</sub>...C<sub>diene</sub> = 2.160 Å) at ZORA- $\omega$ B97X-D/TZ2P//ZORA-BP86-D3(BJ)/TZ2P.

To understand why the  $\Delta E_{\text{int}}$  becomes more stabilizing on going from **1** to **2**, we apply our energy decomposition analysis (EDA),<sup>7</sup> which decomposes the  $\Delta E_{\text{int}}$  into four physically meaningful terms: the classical electrostatic interaction ( $\Delta V_{\text{elstat}}$ ), the Pauli repulsion ( $\Delta E_{\text{Pauli}}$ ) arising from the repulsion between occupied closed-shell orbitals of both deformed reactants, the orbital interaction ( $\Delta E_{\text{oi}}$ ) that accounts for charge transfer and polarization, and the dispersion energy ( $\Delta E_{\text{disp}}$ ). The EDA results reveal that a less destabilizing Pauli repulsion for **2** is the main cause for the more stabilizing interaction energy ( $\Delta \Delta E_{\text{Pauli}} = 14.6$  kcal mol<sup>-1</sup>), see Table 2. The orbital interactions of the DA reactions with **1** and **2** are very similar ( $\Delta \Delta E_{\text{oi}} = 2.2$  kcal mol<sup>-1</sup>) which directly challenges the findings of Karas *et al.*<sup>3</sup>

Now, we explain why the DA reaction of **2** is accelerated by a less destabilizing Pauli repulsion and not by stronger orbital interactions because of the higher energy of the HOMO. First, we examine the origin of the less destabilizing Pauli repulsion for the DA reaction of **2** compared to **1** by performing a Kohn–Sham molecular orbital analysis.<sup>8</sup> The key occupied  $\pi$ -orbitals of **M**, **1**, and **2** are quantified at consistent TS-like geometries. The key occupied  $\pi$ -orbitals are the  $\pi$ -HOMO<sub>M</sub> of **M**, where the 2p<sub>z</sub> atomic orbitals (AOs) of the reactive carbon atoms are in-phase, and the  $\pi$ -MO<sub>diene</sub> of the diene, where all 2p<sub>z</sub> AOs are in-phase. The destabilizing occupied–occupied orbital interaction,  $\pi$ -MO<sub>diene</sub>– $\pi$ -HOMO<sub>M</sub>, sets the trend in Pauli repulsion and the corresponding orbital overlap decreases from 0.07 for **1** to only 0.02 for **2** (Fig. 1a). The main origin of this decrease in orbital overlap is the difference in asynchronicity between these two reactions. As already mentioned, the DA reaction of **2** goes *via* a more asynchronous reaction mode than **1**. As a result, **M** overlaps, due to the longer C...C bond, less at the C <sub>$\alpha$</sub> -atom of **2** than of **1**, manifesting in less Pauli repulsion for the former (Fig. 1b).

Finally, we explain why the orbital interactions for the DA reaction with **1** and **2** are very similar. This contradicts the rationale of Karas *et al.*, who ascribe the lower activation barrier to a gain in antiaromaticity of the diene, which raises the HOMO energy.<sup>3</sup> Fig. 2 shows the molecular orbital diagrams of the DA reaction with **1** and **2**. In line with the work of Karas *et al.*, the normal electron demand (NED) interaction becomes more stabilizing from -29.3 kcal mol<sup>-1</sup> for the DA reaction of **1** to -42.6 kcal mol<sup>-1</sup> for the DA reaction of **2** (Table S2, ESI<sup>†</sup>),<sup>16</sup> due to the destabilization of the HOMO from -8.3 eV for **1** to -1.2 eV for **2** (Fig. 2a). However, simultaneously, the inverse electron demand (IED) between the  $\pi$ -LUMO of the diene and  $\pi$ -HOMO of **M** is suppressed. The IED interaction was weakened from -23.0 kcal mol<sup>-1</sup> for the DA reaction of **1** to -8.4 kcal mol<sup>-1</sup> for **2**.<sup>16</sup> Going from **1** to **2** not only destabilizes the  $\pi$ -HOMO of the diene, but also the  $\pi$ -LUMO of the diene from -1.2 eV for **1** to 4.1 eV for **2** (Fig. 2b), causing the weakening of the IED interaction. Additionally, the orbital overlap decreases from **1** to **2** which originates from the increased asynchronicity (*vide supra*). Thus, the gain in NED interactions is effectively cancelled by the loss in IED interactions and the orbital interactions are similar for the DA



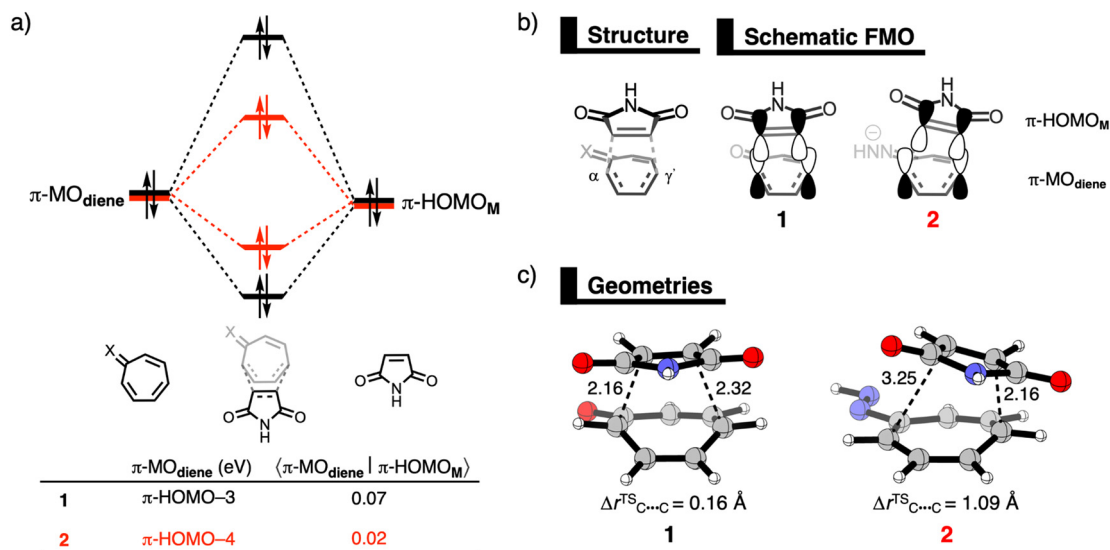


Fig. 1 (a) Molecular orbital diagram with the most significant occupied orbital overlaps; (b) key occupied orbitals (isovalue = 0.03 au); and (c) the structures with key structural information (in Å) of the Diels–Alder reactions between **M** and diene **1** and **2**, computed at consistent TS-like geometries ( $\text{C}_M \cdots \text{C}_{\text{diene}} = 2.160 \text{ \AA}$ ) at ZORA- $\omega$ B97X-D/TZ2P//ZORA-BP86-D3(BJ)/TZ2P.

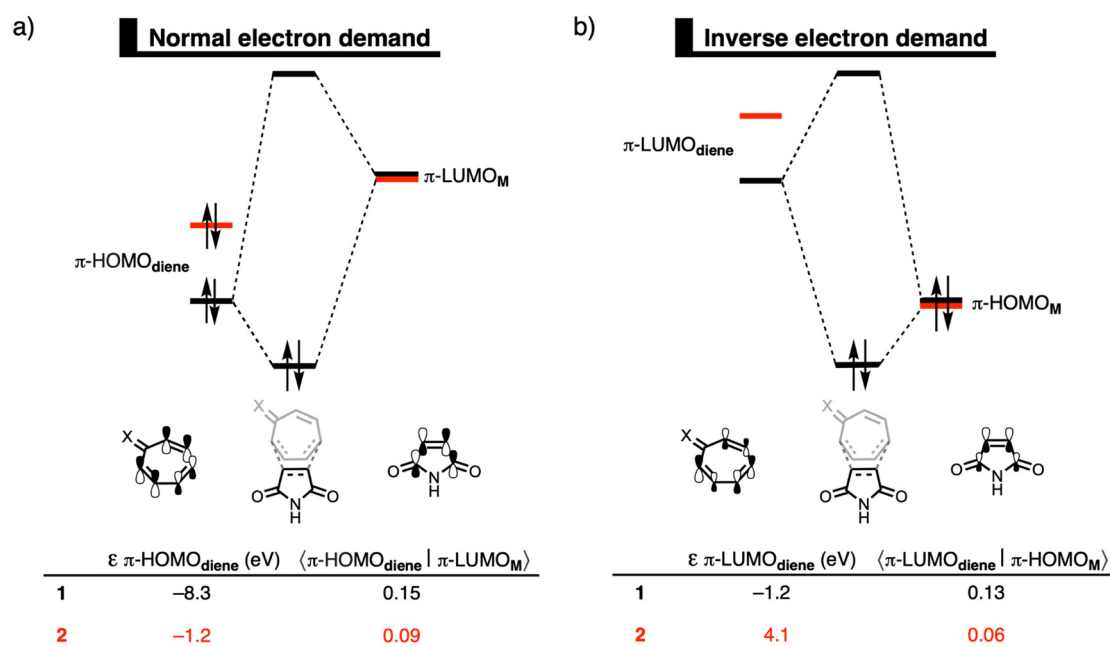


Fig. 2 Kohn–Sham molecular orbital diagrams with orbital energy levels and overlaps for (a) the normal electron demand  $\pi\text{-HOMO}_{\text{diene}}-\pi\text{-LUMO}_M$ ; and (b) the inverse electron demand  $\pi\text{-LUMO}_{\text{diene}}-\pi\text{-HOMO}_M$  of the Diels–Alder reactions between **M** and diene **1** and **2**, computed at consistent TS-like geometries ( $\text{C}_M \cdots \text{C}_{\text{diene}} = 2.160 \text{ \AA}$ ) at ZORA- $\omega$ B97X-D/TZ2P//ZORA-BP86-D3(BJ)/TZ2P.

reactions of **1** and **2**. The *HOMO-raising* effect is, therefore, not the driving force behind DA reactions of tropone hydrazone ions. A correlation between the *HOMO-raising* effect and the accelerated reactivity can be observed, but this does not imply a causality. Thus, caution should be required in demonstrating causal relationships and hence detailed insight into the physical mechanism, as demonstrated in this work, is needed.

To conclude, conversion of tropone into a hydrazone ion analog *via* carbonyl umpolung leads to enhanced Diels–Alder reactivity. Recently, this enhanced reactivity was ascribed to the antiaromatic character of the hydrazone ion analogs, raising the energy of the HOMO.<sup>3</sup> We challenge this frequently used antiaromaticity-induced HOMO-raising rationale and propose that the increased reactivity is not caused by enhanced orbital interactions, but instead by an amplified asynchronicity of the





reaction mode resulting in (i) less destabilizing strain and (ii) a diminished destabilizing Pauli repulsion between the reactants.

## Conflicts of interest

There are no conflicts to declare.

## Notes and references

- (a) V. Nair and K. G. Abhilash, *Synlett*, 2008, 301; (b) S. Frankowski, M. Romaniszyn, A. Skryńska and Ł. Albrecht, *Chem. – Eur. J.*, 2020, **26**, 2120.
- S. Kajigaeshi, S. Matsuoka, S. Kanemasa and M. Noguchi, *J. Heterocycl. Chem.*, 1986, **23**, 49.
- L. J. Karas, A. T. Campbell, I. V. Alabugin and J. I. Wu, *Org. Lett.*, 2020, **22**, 7083.
- (a) S.-L. You, *Asymmetric Dearomatization React.*, Wiley-VCH, 2016; (b) C. Zheng and S.-L. You, *ACS Cent. Sci.*, 2021, **7**, 432; (c) X. Song, Z.-C. Chen, W. Du and Y.-C. Chen, in *Asymmetric Organocatalysis: New Strategies, Catalysts, and Opportunities*, ed. Ł. Albrecht and A. Albrecht, L. Dell'Amico, Wiley-VCH, Weinheim, 2023, **16**, pp. 539–575.
- (a) P. Vermeeren, T. A. Hamlin, I. Fernández and F. M. Bickelhaupt, *Angew. Chem., Int. Ed.*, 2020, **59**, 6201; (b) P. Vermeeren, T. A. Hamlin, I. Fernández and F. M. Bickelhaupt, *Chem. Sci.*, 2020, **11**, 8105; (c) P. Vermeeren, F. Brinkhuis, T. A. Hamlin and F. M. Bickelhaupt, *Chem. – Asian J.*, 2020, **15**, 1167; (d) P. Vermeeren, M. D. Tiezza, M. van Dongen, I. Fernández, F. M. Bickelhaupt and T. A. Hamlin, *Chem. – Eur. J.*, 2021, **27**(41), 10610; (e) S. Yu, F. M. Bickelhaupt and T. A. Hamlin, *ChemistryOpen*, 2021, **10**, 784; (f) S. Portela, J. J. Cabrera-Trujillo and I. Fernández, *J. Org. Chem.*, 2021, **86**, 5317; (g) P. Vermeeren, T. A. Hamlin and F. M. Bickelhaupt, *Chem. – Eur. J.*, 2022, **28**, e202200987; (h) S. Portela and I. Fernández, *Chem. – Asian J.*, 2022, e202201214; (i) S. Portela and I. Fernández, *Tetrahedron Chem.*, 2022, **1**, 100008.
- (a) D. H. Ess and K. N. Houk, *J. Am. Chem. Soc.*, 2008, **130**, 10187; (b) F. M. Bickelhaupt and K. N. Houk, *Angew. Chem., Int. Ed.*, 2017, **56**, 10070; (c) P. Vermeeren, S. C. C. van der Lubbe, C. Fonseca Guerra, F. M. Bickelhaupt and T. A. Hamlin, *Nat. Protoc.*, 2020, **15**, 649; (d) P. Vermeeren, T. A. Hamlin and F. M. Bickelhaupt, *Chem. Commun.*, 2021, **57**, 5880.
- (a) F. M. Bickelhaupt and E. J. Baerends, in *Reviews in Computational Chemistry*, ed. K. B. Lipkowitz and D. B. Boyd, Wiley-VCH, New York, 2000, **1**, pp. 1–86; (b) T. A. Hamlin, P. Vermeeren, C. Fonseca Guerra and F. M. Bickelhaupt, in *Complementary Bonding Analysis*, ed. S. Grabowsky, De Gruyter, Berlin, 2021, **8**, pp. 199–212.
- R. van Meer, O. V. Gritsenko and E. J. Baerends, *J. Chem. Theory Comput.*, 2014, **10**, 4432.
- (a) R. Rüger, M. Franchini, T. Trnka, A. Yakovlev, E. van Lenthe, P. Philipsen, T. van Vuren, B. Klumbers and T. Soini, AMS2021.104, SCM, Theoretical Chemistry, Vrije Universiteit, Amsterdam, 2021; (b) C. Fonseca Guerra, J. G. Snijders, G. te Velde and E. J. Baerends, *Theor. Chem. Acc.*, 1998, **99**, 391; (c) G. te Velde, F. M. Bickelhaupt, E. J. Baerends, C. Fonseca Guerra, S. J. A. van Gisbergen, J. G. Snijders and T. Ziegler, *J. Comput. Chem.*, 2001, **22**, 931.
- (a) A. D. Becke, *Phys. Rev. A: At., Mol., Opt. Phys.*, 1988, **38**, 3098; (b) S. Grimme, J. Antony, S. Ehrlich and H. Krieg, *J. Chem. Phys.*, 2010, **132**, 154104; (c) S. Grimme, S. Ehrlich and L. Goerigk, *J. Comput. Chem.*, 2011, **32**, 1456; (d) E. R. Johnson and A. D. Becke, *J. Chem. Phys.*, 2005, **123**, 024101; (e) E. van Lenthe and E. J. Baerends, *J. Comput. Chem.*, 2003, **24**, 1142; (f) E. van Lenthe, E. J. Baerends and J. G. Snijders, *J. Chem. Phys.*, 1993, **99**, 4597; (g) E. van Lenthe, E. J. Baerends and J. G. Snijders, *J. Chem. Phys.*, 1994, **101**, 9783; (h) E. van Lenthe, A. Ehlers and E. J. Baerends, *J. Chem. Phys.*, 1999, **110**, 8943; (i) P. Vermeeren, M. Dalla Tiezza, M. E. Wolf, M. E. Lahm, W. D. Allen, H. F. Schaefer, T. A. Hamlin and F. M. Bickelhaupt, *Phys. Chem. Chem. Phys.*, 2022, **24**, 18028.
- J.-D. Chai and M. Head-Gordon, *Phys. Chem. Chem. Phys.*, 2008, **10**, 6615.
- (a) X. Sun, T. M. Soini, J. Poater, T. A. Hamlin and F. M. Bickelhaupt, *J. Comput. Chem.*, 2019, **40**, 2227; (b) X. Sun, T. Soini, L. P. Wolters, W.-J. van Zeist, C. Fonseca Guerra, T. A. Hamlin and F. M. Bickelhaupt, *PyFrag 2019*, Vrije Universiteit, Amsterdam, 2019.
- The computed trend in electronic activation barriers is identical to the trend in Gibbs free activation barriers, see Table S1 (ESI).
- Performing this analysis at a consistent point along the reaction coordinate (close to the transition state structures), rather than on the individual transition state structures, assures that the analyses are not skewed by the location of the transition state, see the following reference: T. A. Hamlin, D. Svatoněk, S. Yu, L. Ridder, I. Infante, L. Visscher and F. M. Bickelhaupt, *Eur. J. Org. Chem.*, 2019, 378.
- P. Vermeeren, T. A. Hamlin and F. M. Bickelhaupt, *Phys. Chem. Chem. Phys.*, 2021, **23**, 20095.
- The strength of the normal electron demand (NED) interactions is obtained by performing EDA computations while artificially deleting the virtual orbitals of the diene. Whereas the strength of the inverse electron demand (IED) interactions is obtained by performing EDA computations while artificially deleting the virtual orbitals of M.

